Applied Catalysis B: Environmental 91 (2009) 247–253

Contents lists available at ScienceDirect

Applied Catalysis B: Environmental

journal homepage: www.elsevier.com/locate/apcatb

Aerosol-spay assisted assembly of $Bi_2Ti_2O_7$ crystals in uniform porous microspheres with enhanced photocatalytic activity

Zhenfeng Bian [a], Yuning Huo [a], Yi Zhang [a], Jian Zhu [a], Yunfeng Lu [b,*], Hexing Li [a,*]

[a] Department of Chemistry, Shanghai Normal University, Shanghai 200234, China
[b] Chemical & Biomolecular Engineering Department, University of California, Los Angeles, CA 90095, USA

ARTICLE INFO

Article history:
Received 7 March 2009
Received in revised form 21 May 2009
Accepted 22 May 2009
Available online 6 June 2009

Keywords:
Aerosol-spray assisted assembly
Crystalline $Bi_2Ti_2O_7$
Visible photocatalyst
Uniform porous microspheres
Photodegradation of *p*-chlorophenol (4-CP) and the rhodamine B (RhB)

ABSTRACT

A novel crystalline $Bi_2Ti_2O_7$ in uniform porous microspheres was synthesized by aerosol-spray assisted surfactant self-assembly which displayed strong optical response in visible region owing to the narrow energy gap. During photodegradation of *p*-chlorophenol and rhodamine B under visible light irradiation, this photocatalyst was more active than the $Bi_2Ti_2O_7$ obtained via chemical solution decomposition, apparently owing to the larger surface area and higher crystallization degree which might promote the reactant adsorption and inhibit the charge carrier recombination. The as-prepared $Bi_2Ti_2O_7$ crystal also showed much higher activity than the Bi-doped TiO_2 owing to the low recombination rate between photoelectrons and holes, corresponding to the higher quantum efficiency. Besides, the $Bi_2Ti_2O_7$ crystal was strongly durable and could be used repetitively for more than nine times without significant deactivation, which could be attributed to the high hydrothermal stability against phase transformation and architecture damage.

1. Introduction

Photocatalysis has been under intense investigation due to its potential in hydrogen production by splitting water and the environmental cleaning by degrading organic pollutants [1,2]. Among various semiconductor photocatalysts, the TiO_2 is most frequently employed owing to its low cost, non-toxicity, highly chemical resistance [3,4]. However, pure TiO_2 only becomes active under irradiation with ultraviolet (UV) lights due to its big energy band gap (3.2 eV) [2]. Many efforts have been devoted recently to extend optical response of TiO_2 into visible light region by doping TiO_2 with metals [5], nonmetals [6], semiconductor oxides [7], or/and organic photosensitizers [8] to extend the spectral response into visible region and to improve the quantum efficiency of photocatalysis. Although excellent progress has been made, the practical applications of doped TiO_2 photocatalysts are still quite limited by the low efficiency in utilizing sunlight and the high recombination between photoelectrons and holes. The development of novel non-titania semiconductors with strong absorbance for broad ranged visible lights represents a current trend in photocatalysis [9,10].

It has been reported that the Bi_2O_3/TiO_2 is a visible photocatalyst owing to the narrow energy gap of Bi_2O_3 (2.8 eV) [11,12]. However, the Bi_2O_3 doping intrinsically brings a serious problem of massive charge carrier recombination since Bi species are mainly present in a separated phase (Bi_2O_3) rather than incorporated into the TiO_2 lattice due to its bigger size (103 pm) than the Ti (61 pm) [13]. Meanwhile, the Bi_2O_3 dopants are easily leached off in liquid phase photocatalysis, leading to poor durability. It has been reported that $Bi_2Ti_2O_7$ displayed strong spectral response in visible area owing to the narrow energy gap [14–16]. To date, all the $Bi_2Ti_2O_7$ samples have been synthesized by high-temperature solid phase reactions [17], chemical solution decomposition [18], and sol–gel method [19]. They usually exhibit low surface area, inferior crystallization and poor hydrothermal stability, which limited their applications in photocatalysis due to the poor activity and durability. The flexibility of surfactant self-assembly can efficiently form catalyst-surfactant micellar species into liquid-crystalline mesophases, and stabilize the nanoparticles against aggregation, leading to the improved surface area. Up to now, some materials have been successfully synthesized via with surfactant self-assembly, such as TiO_2 and modified TiO_2 photocatalysts with mesoporous structure [20–23]. In this paper, we report for the first time an aerosol-spray assisted self-assembly of $Bi_2Ti_2O_7$ crystals in uniform porous microspheres, which exhibit high activity and strong durability in liquid phase photocatalytic degradation of organic pollutants owing to the enhanced adsorption for reactant molecules and visible light, the effective inhibition of charge carrier recombination, and the high hydrothermal stability against phase transformation and architecture damage.

* Corresponding authors. Tel.: +86 21 6432 2272; fax: +86 21 6432 2272.
E-mail addresses: luucla@ucla.edu (Y. Lu), hexing-li@shnu.edu.cn (H. Li).

0926-3373/$ – see front matter © 2009 Elsevier B.V. All rights reserved.
doi:10.1016/j.apcatb.2009.05.032

2. Experiment

2.1. Catalyst preparation

Besides F127 ($EO_{106}PO_{70}EO_{106}$, Aldrich), the following reactants (analytical grade) are purchased from Shanghai Chemical Regents Company and used without further purification. In a typical run of synthesis, 8.5 ml $Ti(O–C_4H_9)_4$ (≥99%) was added dropwise into 40.0 ml aqueous solution containing certain amount of F127, 12.1 g $Bi(NO_3)_3{\cdot}5H_2O$ (≥98%) and 60.0 ml acetic acid (≥99.5%). Then, in a self-designed aerosol-spraying reactor (Fig. S1), the solution was atomized into aerosol droplets, followed by passing through a quartz glass tube at a given temperature with the N_2 carrier gas. The solid product was filtered and collected, followed by calcination at a desired temperature for 6 h. The as-prepared samples were denoted as BTO-X-Y-Z, where X, Y, and Z refer to the amount of F127 (g), aerosol-spraying temperature (°C), and calcination temperature (°C), respectively. For comparison, the conventional $Bi_2Ti_2O_7$ was also prepared via chemical solution decomposition at 600 °C [19], and denoted as BTO-CSD. Meanwhile, the Bi-doped TiO_2 with Bi/Ti molar ratio of 1.0% was synthesized by EISA-assisted sol–gel route [12], followed by calcination at 500 °C for 6 h. The P25 TiO_2 was commercially available and used without further treatment.

2.2. Characterizations

The sample composition was determined by either energy dispersive X-ray spectroscopy (EDX, JEM-2100) or inductively coupled plasma (ICP, Varian VISTA-MPX). The structure was examined by Fourier transform infrared spectrometer (FTIR, NEXUS 470), X-ray diffraction (XRD, Rigacu Dmax-3C). Surface morphology was observed by scanning electron microscopy (SEM, JEOL JSM-6380LV) and transmission electronic microscopy (TEM, JEM-2010). X-ray photoelectron spectroscopy (XPS, Versa Probe PHI 5000) was employed to determine surface electronic states. The shift of the binding energy due to relative surface charging was corrected using the C_{1S} level at 284.8 eV as an internal standard. N_2 adsorption–desorption isotherms were measured on a Quantachrome NOVA 4000e at 77 K. The Brunauer–Emmett–Teller (BET) method was used to calculate the specific surface area (S_{BET}) and the Barrett–Joyner–Halenda (BJH) model was used to calculate pore volume (V_P). The thermal stability was investigated by a thermogravimetric analyzer (DTG-60H, 10 °C/min heating rate). The light absorption ability was analyzed by both UV–vis diffuse reflectance spectra (DRS, MC-2530) and photoluminescence spectra (PLS, Varian Cary-Eclipse 500).

2.3. Activity test

The *p*-chlorophenol (4-CP) photodegradation was carried out at 30 °C in a self-designed quartz reactor containing 50.0 ml of 1.0×10^{-4} M 4-CP and 0.10 g catalyst. The mixture was allowed to stir for enough time (>1 h) under dark for reaching adsorption equilibrium. Then, the photocatalytic reaction was initiated by irradiating with one 500 W Xe lamp (CHF-XM500, light intensity = 600 mW/cm^2) located 18 cm above the solution surface. To make sure that the photocatalytic reaction was really driven by visible lights, the radiation with wavelength less than 420 nm were cut off by a glass filter (JB-420). The reaction system was stirred vigorously at 800 rpm to eliminate diffusion effect. After reaction for 6 h, the unreacted 4-CP was analyzed by a UV spectrophotometer (UV 7504/PC) at characteristic wavelength of 224 nm [24] to determine degradation yield. The rhodamine B (RhB) photodegradation was carried out in the similar procedure by using 50.0 ml of 1.0×10^{-5} M RhB instead of 4-CP. After reaction for 3 h, the unreacted RhB was analyzed by a UV spectrophotometer at characteristic wavelength of 554 nm [25]. Except for CO_2, no organic products were detected by either UV–vis spectroscopy or HPLC, indicating the thorough mineralization of 4-CP and RhB under the present conditions, which was further confirmed by TOC analysis. Preliminary tests demonstrated that no significant change in either 4-CP or RhB concentration was detected if the reaction mixture was allowed to stir for 6 or 3 h in the absence of light source, indicating that the possibility of the adsorption could be excluded. Meanwhile, only less than 3% 4-CP and 7% RhB decomposed after reaction for 6 or 3 h in the absence of the photocatalyst and thus could be neglected in comparison with degradation yield resulting from photocatalysis. The reproducibility of the results was checked by repeating each reaction at least three times and was found to be within acceptable limits (±5%).

3. Results and discussion

The FTIR spectrum (Fig. 1) revealed that, besides two peaks at 1630 and 3400 cm^{-1} indicative of surface adsorbed hydroxyl groups [26], the BTO-3-350-500 sample displayed two additional peaks around 489 and 582 cm^{-1} due to the vibrations from Bi–O [27] and Ti–O bonds [28], respectively. Unlike the BTO-3-350 sample without calcination, no other peaks indicative of C–O–C and C–H bonds were observed, suggesting the complete removal of F127 surfactant and other organic residues [29], which was further confirmed by TG/DTA analysis. As shown in Fig. 2, the BTO-3-350 exhibited two exothermic peaks around 275 and 358 °C with weight loss around 30%, while the BTO-3-350-500 displayed no significant weight loss and exothermic peaks.

According to ICP and EDX analysis, the composition of BTO-3-350-500 was determined as $Bi_2Ti_2O_7$. Meanwhile, the XPS spectra in Bi_{4f}, Ti_{2p} and O_{1s} levels (Fig. 3) were consistent with those observed in the $Bi_2Ti_2O_7$ [30–32]. No other peaks indicative metallic Bi [30], TiO_2 [31], Bi_2O_3 [33], and $Bi_4Ti_3O_{12}$ [34] were observed, suggesting that the sample was pure. The XRD patterns in Fig. 4 demonstrated that the Bi-doped TiO_2 exhibited only diffractions indicative of anatase. In comparison with the undoped TiO_2, no significant shift of the diffractional peaks occurred, indicating the Bi species were present mainly in the separated Bi_2O_3 phase rather than incorporated into the TiO_2 lattice [12]. The failure in observing diffractions characteristic of Bi species was ascribed to the low Bi-content. Both the BTO-3-350-500 and the BTO-CSD displayed similar XRD patterns indicative of $Bi_2Ti_2O_7$

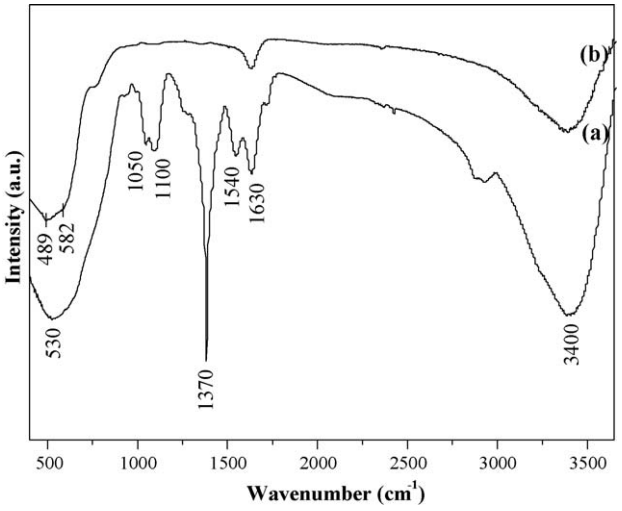

Fig. 1. FTIR spectra of (a) BTO-3-350 and (b) BTO-3-350-500 samples.

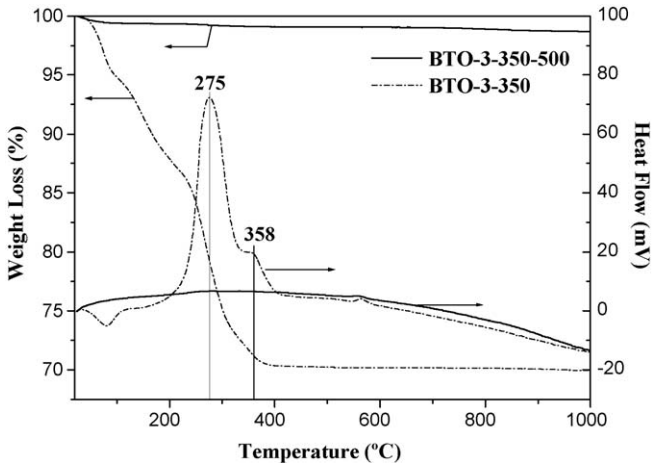

Fig. 2. TG/DTA curves of BTO-3-350 and BTO-3-350-500 samples.

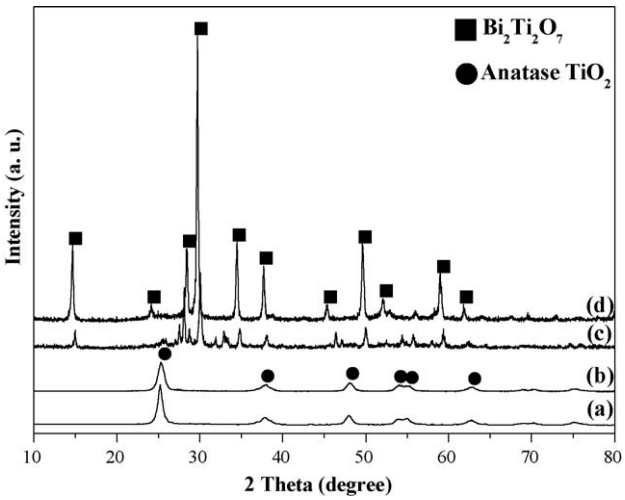

Fig. 4. XRD patterns of (a) undoped TiO_2, (b) Bi-doped TiO_2 (Bi_2O_3/TiO_2), (c) BTO-CSD, and (d) BTO-3-350-500 samples.

crystals with high purity since no significant XRD diffractions characteristic of either the TiO_2 or the Bi_2O_3 were observed [18]. Based on the principal peak (4 4 4), the lattice constant (a), calculated from equation of $a = d_{hkl}(h^2 + k^2 + l^2)^{1/2}$, was found to be 20.68 Å, which was in good agreement with pyrochlore-type crystal structure of $Bi_2Ti_2O_7$ (see Fig. S2) [16,18,35].

As shown in Fig. 5, the SEM and TEM images demonstrated that the BTO-3-350-500 was present in uniform porous microspheres with average diameter around 850 nm. The HRTEM image confirmed the highly crystallized $Bi_2Ti_2O_7$, corresponding to the ordered lattice fringes with an inter-planar space of 5.95 Å indicative of (2 2 2) plane. The N_2 adsorption–desorption isotherm (Fig. S3) also displayed the porous structure at about $P/P_0 = 0.7 \sim 0.9$ [36], which could be attributed to the self-assembly of F127 surfactant. Based on the adsorption branches, the surface area (S_{BET}) and pore volume (V_P) were calculated by applying the Barrett–Joyner–Halenda (BJH) model (see Table 1).

Based on the mechanism of aerosol-spraying synthesis of porous silica [37], Fig. 6 schematically depicts the formation of porous microspheres of the crystalline $Bi_2Ti_2O_7$ by the aerosol-spray assisted self-assembly. Starting with an aqueous solution containing Ti^{4+}, Bi^{3+} and F127 surfactant, the aerosol apparatus atomized the solution into droplets that underwent drying and solidification steps generating microspheres. During this process, solvent evaporation enriched surfactant molecules, Ti^{4+} and Bi^{3+} ions from the N_2–liquid interface of the droplet towards its interior, together with the partial hydrolysis of Ti^{4+} and Bi^{3+} (see reactions (1) and (2)). Subsequent cross-condensation between Ti^{4+} and Bi^{3+} (see reaction (3)) during the drying and heating steps yielded the $Bi_2Ti_2O_7$ nanoparticles, followed by aggregating into microspheres [38]. Calcination at high temperature induced the crystallization of $Bi_2Ti_2O_7$, together with the construction of porous network due to removing surfactant template and other organic residues.

Fig. 7 shows the XRD patterns of BTO-X-Y-Z samples obtained under different conditions. In the absence of F127 surfactant, the BTO-0-350-500 displayed (0 0 2) diffraction characteristic of $Bi_4Ti_3O_{12}$ impurity (JCPDS 35-795). According to the XRD patterns of BTO samples prepared at different amount of F127 (see Fig. S4), the increase of F127 amount from 0 to 3.0 g could inhibit the $Bi_4Ti_3O_{12}$ formation and also enhance the crystallization degree of $Bi_2Ti_2O_7$. However, further increase of F127 amount could decrease the crystallization degree of $Bi_2Ti_2O_7$, possibly due to the disturbing effect on crystallization process. The crystallization degree of the $Bi_2Ti_2O_7$ increased with the elevated aerosol-spraying temperature and calcination temperature. However, very high aerosol-spraying temperature or calcination temperature

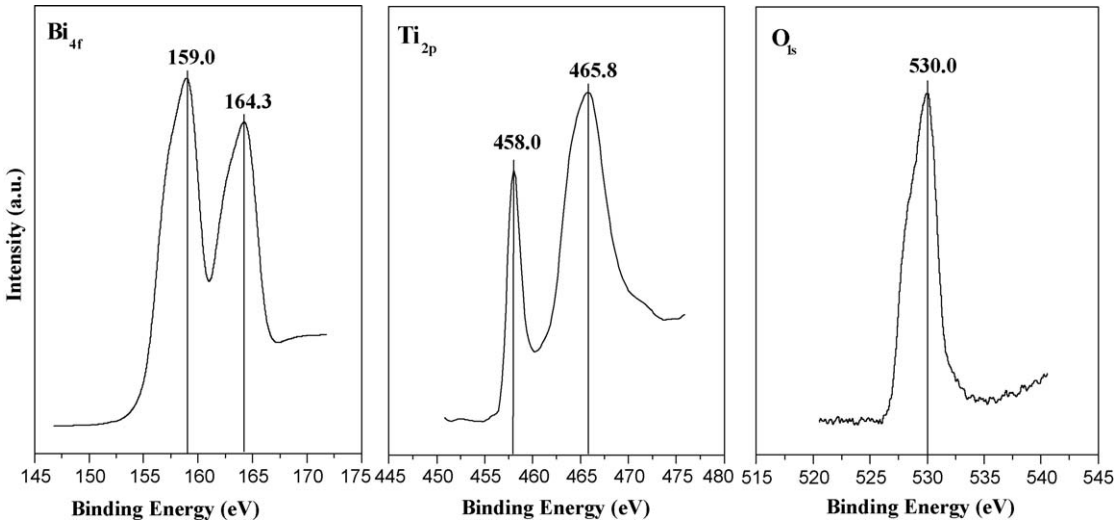

Fig. 3. XPS spectra of the BTO-3-350-500 sample.

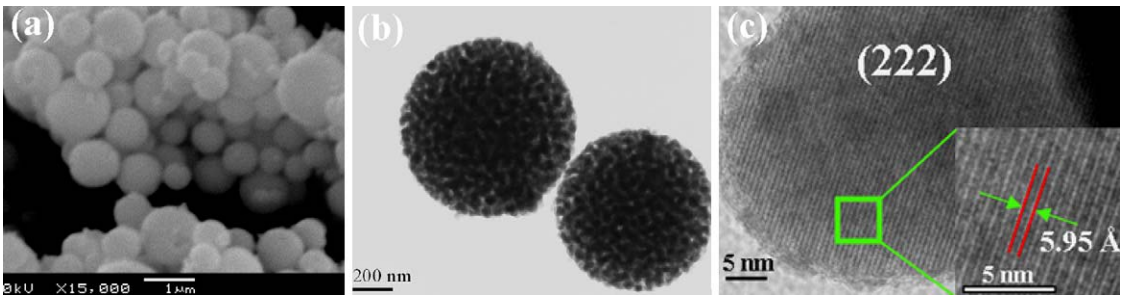

Fig. 5. (a) SEM, (b) TEM, and (c) HRTEM images of the BTO-3-350-500 sample.

Table 1
Structure parameters and photocatalytic activity of different samples[a].

Sample	Crystallite size (nm)	S_{BET} (m^2/g)	V_P (m^3/g)	Degradation (%)	
				4-CP	RhB
BTO-3-300-500	34	12	0.11	35	70
BTO-3-350-500	40	17	0.15	57	91
BTO-3-450-500	26	34	0.17	20	70
BTO-3-350-450	20	47	0.20	40	83
BTO-3-350-550	36	15	0.09	30	71
BTO-3-350-750	29	5.4	0.03	12	56
BTO-0-350-500	33	8.9	0.06	19	78
BTO-CSD	36	4.7	0.03	10	64
Bi_2O_3/TiO_2	19	37	0.17	27	59
P 25 TiO_2	27	45	0.20	10	32
Used BTO-3-350-500[b]	34	12	0.07	/	88

[a] Reaction conditions: 0.10 g catalyst, 50.0 ml solution of 1.0×10^{-4} M 4-CP or 1.0×10^{-5} M RhB, reaction temperature = 30 °C, stirring rate = 800 rpm, one 500 W Xe lamp (light intensity = 600 mW/cm^2, wavelength > 420 nm), reaction time (4-CP) = 6 h, reaction time (RhB) = 3 h.
[b] The photocatalyst after being used repetitively for nine times.

induced a phase transformation from $Bi_2Ti_2O_7$ to $Bi_4Ti_3O_{12}$, together with the decrease of crystallization degree of the $Bi_2Ti_2O_7$ (see the XRD patterns attached to Fig. 7). The optimum aerosol-spraying temperature and calcination temperature were determined as 350 and 500 °C, respectively. Based on the principal (4 4 4) diffraction, the crystallite size was calculated using Scherrer equation ($D = K\lambda/\beta \cos\theta$). As shown in Table 1, increase of either the aerosol-spraying temperature or the calcination temperature promoted crystal growth, leading to the increased crystallite size. The increased aerosol-spraying temperature also promoted self-assembly of porous structure, leading to the enhanced S_{BET} and V_P. However, the increase of calcination temperature might damage the porous structure, which could account for the decrease in S_{BET} and V_P. Further increase in the aerosol-spraying temperature caused a phase transformation, leading to the decrease of crystallite size and thus, the increase of S_{BET}. However, the S_{BET} decreased abruptly at high calcination temperature, obviously due to collapse of porous structure. The BTO-3-350-500 exhibited bigger crystallite size than the BTO-0-350-500. On one hand, the presence of F127 surfactant could enhance crystallization degree of $Bi_2Ti_2O_7$ (see Fig. S4), leading to the bigger crystallite size of BTO-3-350-500. On the other hand, the phase transformation from $Bi_2Ti_2O_7$ to $Bi_4Ti_3O_{12}$ occurred in the absence of F127 surfactant, which could also account for the decrease in the crystallite size of BTO-0-350-500. Though the bigger crystallite size, BTO-3-350-500 still exhibited higher S_{BET} than BTO-0-350-500, which could mainly be attributed to the formation of porous structure induced by the self-assembly of F127 surfactant (see Fig. S3), corresponding to the enhanced V_P.

The UV–vis DRS spectra (Fig. 8) revealed that the undoped TiO_2 displayed no significant absorbance of visible light, while the BTO-3-350-500, BTO-3-350-500 and the Bi-doped TiO_2 samples showed strong spectral response in visible region. According to the UV–vis DRS spectra, the band energy gap could be calculated by using $(\alpha h\upsilon)^n = k(h\upsilon - E_g)$, where α is the absorption coefficient, k is the

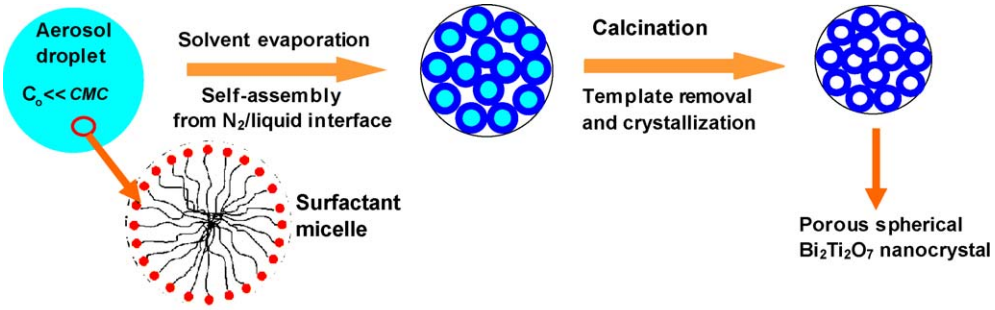

$$\equiv Ti(OR) + H_2O \rightarrow \equiv Ti(OH) + ROH \qquad \text{Hydrolysis (1)}$$

$$Bi^{3+} + H_2O \rightarrow =Bi(OH) + H^+ \qquad \text{Hydrolysis (2)}$$

$$=Bi(OH) + (HO)Ti\equiv \rightarrow =Bi\text{-}O\text{-}Ti\equiv + H_2O \qquad \text{Cross-condensation (3)}$$

Fig. 6. Schematically illustrating the formation of crystalline $Bi_2Ti_2O_7$ porous microspheres by the aerosol-spray assisted self-assembly. The symbols (=) and (≡) in reaction formula represent two or three covalent bonds, respectively.

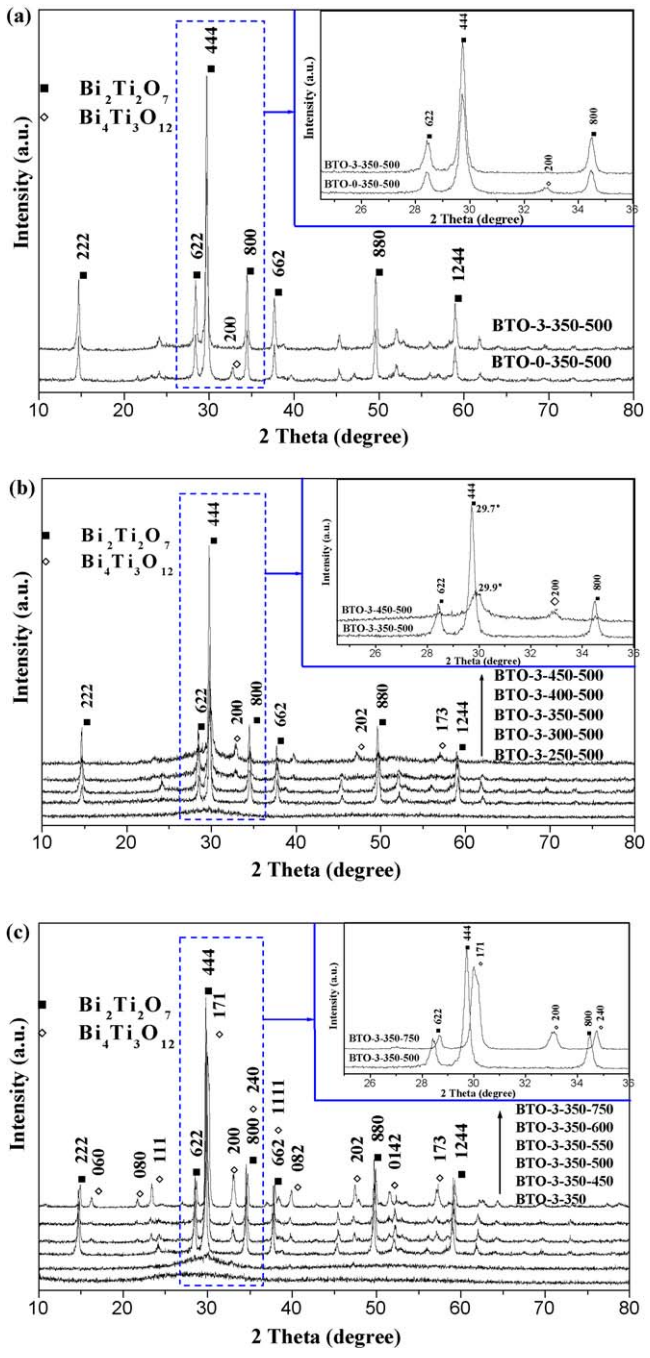

Fig. 7. XRD patterns of the BTO samples showing effects of (a) the F127, (b) the aerosol-spraying temperature, and (c) the calcination temperature.

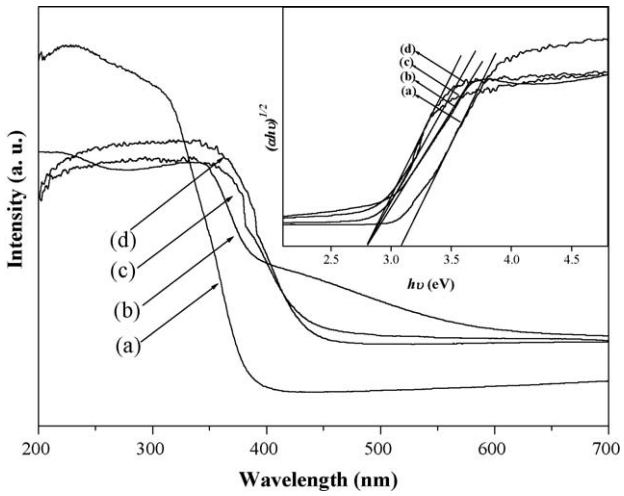

Fig. 8. UV–vis DRS spectra and the optical absorption edges (inset) of (a) undoped TiO_2, (b) Bi-doped TiO_2 (Bi_2O_3/TiO_2), (c) BTO-3-350-450, and (d) BTO-3-350-500.

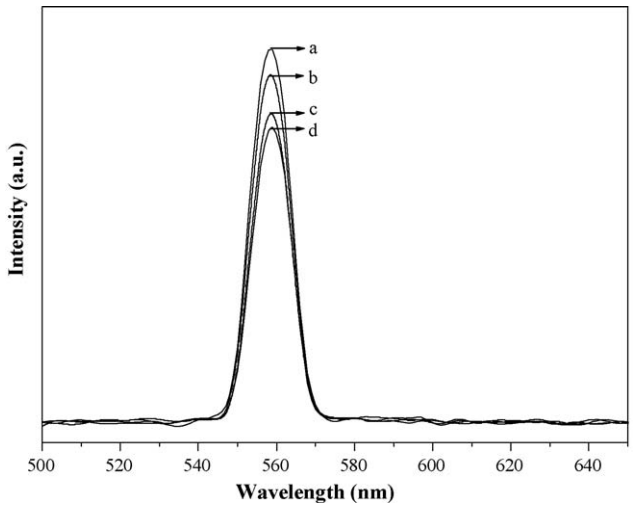

Fig. 9. PL spectra with the excitation wavelength of 280 nm. (a) Bi-doped TiO_2 (Bi_2O_3/TiO_2), (b) BTO-3-350-550, (c) BTO-3-350-450, and (d) BTO-3-350-500.

parameter that related to the effective masses associated with the valence and conduction bands, n is 1/2 for a direct transition, $h\upsilon$ is the absorption energy, and E_g is the band-gap energy [39,40]. Plotting $(\alpha h\upsilon)^{1/2}$ vs $h\upsilon$ gave the extrapolated intercept corresponding to the E_g values. From the optical absorption edges attached in Fig. 8, the band gaps (E_g) of undoped TiO_2, Bi-doped TiO_2, BTO-3-350-450, and BTO-3-350-500 were determined as 3.1, 2.8, 2.8, and 2.8 eV, respectively. The low E_g of the Bi-doped TiO_2 belonged to pure Bi_2O_3 [11], while the low E_g of BTO was resulted from the inherent conduction and valance bands of the $Bi_2Ti_2O_7$ semiconductor [17,18].

PL emission spectra have been widely used to investigate the efficiency of charge carrier trapping, migration, and transfer in order to understand the fate of electron-hole pairs in semiconductor particles since PL emission results from the recombination of free carrier. The stronger PL peak around 550 nm corresponded to the higher charge carrier recombination rate. [41] As shown in Fig. 9, the Bi-doped TiO_2 displayed the strongest intensity of the PL peak, which could be attributed to the high recombination rate between photoelectrons and holes in the Bi_2O_3, taking into account that the Bi species were present in separated phase of Bi_2O_3 rather than incorporated into the TiO_2 lattice. The BTO-3-350-500 exhibited lower intensity of the PL peak than the BTO-3-350-450 obtained at low calcination temperature since the enhanced crystallization degree facilitated the rapid transfer of photoelectrons and thus, inhibited their recombination with photo-induced holes [42]. Meanwhile, the BTO-3-350-550 also showed stronger PL peak than the BTO-3-350-500, corresponding to the easer photoelectron-hole recombination since calcination at very high temperature caused a decrease in the crystallization degree of $Bi_2Ti_2O_7$ due to the phase transformation from $Bi_2Ti_2O_7$ to $Bi_4Ti_3O_{12}$.

Photodegradation of *p*-chlorophenol (4-CP) and rhodamine B (RhB) under visible irradiation were chosen to evaluate the catalytic performances, since 4-CP and RhB represented typical

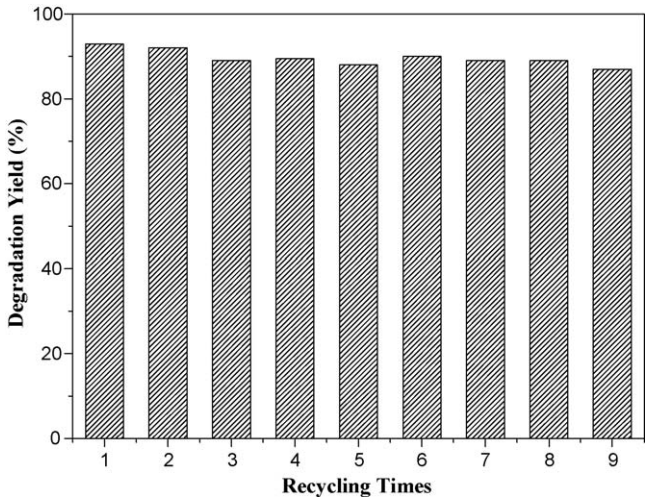

Fig. 10. Recycling tests of the BTO-3-350-500 photocatalyst. Reaction conditions: 0.10 g catalyst, 50.0 ml solution of 1.0×10^{-5} M RhB, reaction temperature = 30 °C, stirring rate = 800 rpm, one 500 W Xe lamp (light intensity = 600 mW/cm^2, wavelength > 420 nm). Each run of photocatalytic reactions lasted for 3 h.

organic pollutants in the wastewater from chemistry and dyeing industries. As shown in Table 1, the P25 TiO_2 exhibited very low activity in degradation of either *p*-chlorophenol (4-CP) or rhodamine B (RhB) since it could not be activated by visible lights due to its big energy gap (3.1 eV). Although the same E_g and the higher S_{BET}, the Bi-doped TiO_2 exhibited much lower activity than the BTO-3-350-500, which could be mainly attributed to the charge carrier recombination, leading to the low quantum efficiency [41]. Meanwhile, the BTO-3-350-500 was more active than the BTO-CSD obtained via traditional method. On one hand, the high S_{BET} promoted the adsorption for reactant molecules. On the other hand, the high crystallization degree of the $Bi_2Ti_2O_7$ facilitated the rapid transfer of photo-induced electrons from bulk to the surface and thus, could effectively inhibit the photoelectron-hole recombination, leading to the high quantum efficiency [42].

Table 1 also showed the effects of preparation conditions on the activity. Firstly, the BTO-3-350-500 was much more active than BTO-0-350-500. The promoting effect of F127 could be attributed to both the enhancement of S_{BET} and the inhibition of phase transformation from $Bi_2Ti_2O_7$ to $Bi_4Ti_3O_{12}$, taking into account that the $Bi_4Ti_3O_{12}$ was inactive under visible irradiation due to the big energy band gap (3.1 eV) [17]. Secondly, the increase of aerosol-spraying temperature from 300 to 350 °C promoted the activity owing to the slight increase in S_{BET} [4,5] and more importantly, the enhanced crystallization degree of $Bi_2Ti_2O_7$ [42]. However, very high aerosol-spraying temperature (> 350 °C) was harmful for the activity due to the phase transformation from $Bi_2Ti_2O_7$ to $Bi_4Ti_3O_{12}$. The effect of calcination temperature on the activity was similar to that of the aerosol-spraying temperature. From 450 to 500 °C, the activity increased owing to the enhanced crystallization degree of $Bi_2Ti_2O_7$. Further increase in calcination temperature led to decreased activity due to phase transformation from $Bi_2Ti_2O_7$ to $Bi_4Ti_3O_{12}$.

Besides the high activity, the BTO-3-350-500 also displayed strong durability. As shown in Fig. 10, the BTO-3-350-500 could be used repetitively for more than nine times with only 3% decrease in activity. This could be attributed to the excellent hydrothermal stability of the $Bi_2Ti_2O_7$. The XRD pattern (Fig. S3) demonstrated that the BTO-3-350-500 still displayed well crystallized $Bi_2Ti_2O_7$ without significant phase transformation after being used for nine times. Meanwhile, the attached TEM image clearly showed the well preservation of uniform porous microspheres. The used BTO-3-350-500 showed slight decrease in V_P and S_{BET} (see Table 1) mainly due to blockage of pore channels by adsorbed RhB molecules, which could be easily recovered by extracting in ethanol solution.

4. Conclusions

This work provides a simple approach to prepare $Bi_2Ti_2O_7$ crystals in uniform porous microspheres by aerosol-spray assisted self-assembly. This material displays high purity, large surface area, narrow energy gap, and high degree of crystallization, leading to high photocatalytic activity under irradiation with visible light. Besides, it also shows strong durability owing to the excellent hydrothermal stability against phase transformation and collapse of porous structure. Other semiconductors could also be designed based on present method, which offers more opportunities for developing new phoyocatalytic, optic, and photoelectric materials with promising properties.

Acknowledgments

This work was supported by National Natural Science Foundation of China (20825724), Shanghai Government (S30406, 07dz22303, 09YZ162, 0852nm01000) and Shanghai Normal University (DZL807, SK200838).

Appendix A. Supplementary data

Supplementary data associated with this article can be found, in the online version, at doi:10.1016/j.apcatb.2009.05.032.

References

[1] A.J. Esswein, D.G. Nocera, Chem. Rev. 107 (2007) 4022.
[2] M. Anpo, M. Takeuchi, J. Catal. 216 (2003) 505.
[3] S. Usseglio, A. Damin, D. Scarano, S. Bordiga, A. Zecchina, C. Lamberti, J. Am. Chem. Soc. 129 (2007) 2822.
[4] M. Anpo, S. Dohshi, M. Kitano, Y. Hu, M. Takeuchi, M. Matsuoka, Annu. Rev. Mater. Res. 35 (2005) 1.
[5] X.B. Chen, S.S. Mao, Chem. Rev. 107 (2007) 2891.
[6] H.X. Li, J.X. Li, Y.N. Huo, J. Phys. Chem. B 110 (2006) 1559.
[7] J.C. Yu, L. Wu, J. Lin, P. Li, Q. Li, Chem. Commun. (2003) 1552.
[8] D. Zhao, C.C. Chen, Y.F. Wang, W.H. Ma, J.C. Zhao, T. Rajh, L. Zang, Environ. Sci. Technol. 42 (2008) 308.
[9] H.G. Kim, D.W. Hwang, J.S. Lee, J. Am. Chem. Soc. 126 (2004) 8912.
[10] T. Kako, Z.G. Zou, M. Katagiri, J.H. Ye, Chem. Mater. 19 (2007) 198.
[11] Y. Bessekhouad, D. Robert, J.V. Weber, Catal. Today 101 (2005) 315.
[12] Z.F. Bian, J. Zhu, S.H. Wang, Y. Cao, X.F. Qian, H.X. Li, J. Phys. Chem. C 112 (2008) 6258.
[13] S. Rengaraj, X.Z. Li, P.A. Tanner, Z.F. Pan, G.K. Pang, J. Mol. Catal. A: Chem. 247 (2006) 36.
[14] S.J. Henderson, O. Shebanova, A.L. Hector, P.F. McMillan, M.T. Weller, Chem. Mater. 19 (2007) 1712.
[15] X.N. Yang, B.B. Huang, H.B. Wang, S.X. Shang, W.F. Yao, J.Y. Wei, Mater. Lett. 58 (2004) 3725.
[16] R. Seshadri, Solid State Sci. 8 (2006) 259.
[17] A. Kudo, S. Hijii, Chem. Lett. 83 (1999) 1103.
[18] W.F. Yao, H. Wang, Appl. Catal. A: Gen. 259 (2004) 29.
[19] W.F. Su, Y.T. Lu, Mater. Chem. Phys. 80 (2003) 632.
[20] H. Choi, A.C. Sofranko, D.D. Dionysiou, Adv. Funct. Mater. 16 (2006) 1067.
[21] H. Choi, M.G. Antoniou, M. Pelaez, A.A. Cruz, J.A. Shoemaker, D.D. Dionysiou, Environ. Sci. Technol. 41 (2007) 7530.
[22] E. Stathatos, T. Petrova, P. Lianos, Langmuir 17 (2001) 5025.
[23] H.X. Li, Z.F. Bian, J. Zhu, Y.N. Huo, H. Li, Y.F. Lu, J. Am. Chem. Soc. 129 (2007) 4538.
[24] S. Sakthivel, H. Kisch, Angew. Chem. Int. Ed. 42 (2003) 4908.
[25] J. Ryu, W. Choi, Environ. Sci. Technol. 42 (2008) 294.
[26] V. Parvanova, J. Therm. Anal. Calorim. 86 (2006) 443.
[27] V. Dimitrov, Y. Dimitriev, A. Montenero, J. Non-Cryst. Solids 180 (1994) 51.
[28] Y.M. Kan, X.H. Jin, G.J. Zhang, P.L. Wang, Y.B. Cheng, D.S. Yan, J. Mater. Chem. 14 (2004) 3566.
[29] W.D. Ma, H. Xu, C. Wang, S.F. Nie, W.S. Pan, Int. J. Pharm. 350 (2008) 247.
[30] M.W. Chu, M. Ganne, M.T. Caldes, L. Brohan, J. Appl. Phys. 91 (2002) 3178.
[31] G.W. Hwang, W.D. Kim, Y. Min, Y.J. Cho, C.S. Hwang, J. Electrochem. Soc. 153 (2006) 20.

[32] B.V.R. Chowdari, Z. Rong, Solid State Ionics 90 (1996) 151.
[33] Y.A. Teterin, K.E. Ivanov, A.Y. Teterin, A.M. Lebedev, I.O. Utkin, L. Vukchevich, J. Electron. Spectrosc. Relat. Phenom. 101 (1999) 401.
[34] C. Jovalekić, M. Pavlović, Appl. Phys. Lett. 72 (1998) 1051.
[35] S. Shimada, K. Kodaira, T. Matsushita, J. Cryst. Growth 41 (1977) 317.
[36] J.N. Kondo, K. Domen, Chem. Mater. 20 (2008) 835.
[37] C.J. Brinker, Y.F. Lu, A. Sellinger, H.Y. Fan, Adv. Mater. 11 (1999) 579.
[38] Y. Lu, R. Guanguili, C. Drewien, M. Anderson, C. Brinker, W. Gong, Y. Guo, H. Soyez, B. Dunn, M. Huang, J. Zink, Nature 389 (1997) 364.
[39] M. Yoon, M. Seo, C. Jeong, J.H. Jang, K.S. Jeon, Chem. Mater. 17 (2005) 6069.
[40] L. Li, Y. Yang, X. Huang, G. Li, L. Zhang, J. Phys. Chem. B 109 (2005) 12394.
[41] L.Q. Jing, Y.C. Qu, B.Q. Wang, S.D. Li, B.J. Jiang, L.B. Yang, W. Fu, H.G. Fu, J.Z. Sun, Sol. Energy Mater. Sol. Cells 90 (2006) 1773.
[42] B. Ohtani, Y. Ogawa, S.I. Nishimoto, J. Phys. Chem. B 101 (1997) 3746.